Fracture Mechanics of Concrete and Concrete Structures -
Recent Advances in Fracture Mechanics of Concrete - B. H. Oh, et al.(eds)

Fracture analysis of strain hardening cementitious composites by means of discrete modeling of short fibers

M. Kunieda, K. Kozawa, N. Ueda & H. Nakamura
Dept. of Civil Engineering, Nagoya University, Nagoya, Japan

ABSTRACT: There are a wide variety of short fiber reinforced cement composites, such as strain hardening and multiple fine cracking in tension. Quantitative material design methods considering the properties of matrix, fiber and their interface should be established. This paper introduces numerical model by means of three-dimensional meso-scale analysis (i.e. matrix, fiber and their interface are discretized respectively.), to simulate the tensile fracture including strain hardening and multiple fine cracking. The fibers with specific length and diameter have been arranged within the specimen, and loading tests in analysis have been also carried out to compare with experimental results. It was clarified that the proposed model can be roughly simulated the tensile failure of high strength Strain Hardening Cementitious Composites (SHCC) includes crack patterns. And the effects of matrix strength, its variation and fiber distribution on the tensile fracture were numerically investigated.

1 INTRODUCTION

The performance of short fiber reinforced cementitious composites has been enhanced in recent years, with a variety of material design methods being proposed to achieve the required mechanical performance. Typical material is Strain Hardening Cementitious Composites (SHCC), such as Engineered Cementitious Composites (ECC) developed by Li, V.C. (1993). The material was designed based on micro mechanics principle. The effects of fiber orientation and heterogeneity due to the fiber distribution cannot be, however, investigated in ordinary material design concepts directly. And a new material using hybrid fiber (i.e. combination of different fiber lengths or fiber types) has been also proposed.

Bolander & Saito (1997), for instance, conducted 2-D analysis in which short fibers were discretized as beam elements to examine tensile fracture of fiber reinforced concrete parametrically, the effect of the fiber distribution on the mechanical performance of the resulting composite. Kunieda et al. (2008) proposed three-dimensional meso-scale analysis for SHCC based on a Rigid-Body-Spring Model (RBSM) (Kawai 1978) to elucidate the tensile fracture of ordinary SHCC (ECC) with PVA fibers. And the proposed model can well simulate the tensile fracture of SHCC. However, the applicability of the model to other type of SHCCs (e.g. high strength) should be clarified.

This paper presents the analytical results of high strength SHCC by means of discrete modeling of short fibers. In order to interpret the fracture mechanism (strength and strain capacity, crack pattern), parametric analyses concerning variation of matrix strength and fiber distribution was conducted.

2 OUTLINE OF PROPOSED MODEL

2.1 *Outline of RBSM*

Figure 1 shows an example of a pair of elements (Voronoi cells in the Fig.) composing the element stiffness matrix in the RBSM (Bolander & Berton 2004). These elements were assumed to be rigid bodies, while setting 6 degrees of freedom for each rigid element. Six springs were placed on each boundary plane of each cell, in the normal (1 spring) and tangential (2 springs) to the boundaries and rotational directions (3 springs). The material properties (tensile strength, elastic modulus, and fracture energy) of the matrix were adopted as the mechanical properties of the normal and tangential springs, whereas the mechanical properties of the rotational springs were assumed based on the literature (Bolander & Berton 2004). Note that fracture was evaluated using the crack band based on the distance between each element h to minimize the effect of the discretization on the cracking properties (Thomure et al. 2001).

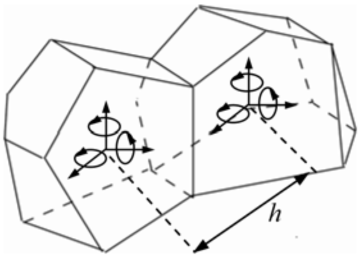

Figure 1. Elements and defined degrees of freedom.

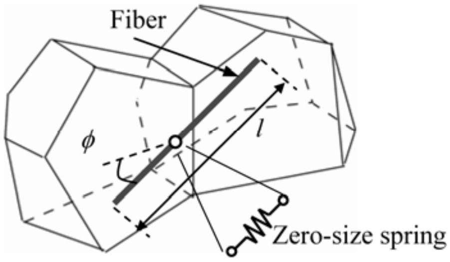

Figure 2. Fiber location and zero-size spring.

2.2 *Modeling of fiber action before cracking of cement matrix*

Before cracking of cement matrix, the stress borne by fibers was calculated based on the shear lag theory by Cox (1952). Cox expressed the tensile stress distribution acting on fibers in the matrix as Equation 1. The authors therefore expressed the reinforcing effect of fibers before cracking by calculating the tensile stress of fibers using Equation 1.

$$\sigma_f = E_f \varepsilon_m \left\{ 1 - \frac{\cosh \beta(l/2 - x)}{\cosh \beta(l/2)} \right\} \tag{1}$$

where σ_f = tensile stress of fibers (MPa), E_f = elastic modulus of fibers (MPa), ε_m = strain of matrix in the direction of the fiber, l = fiber length (mm), x = distance from the end of fiber (mm), and β = constant determined by material constant of matrix and fibers (1.0 in this study).

2.3 *Modeling of fiber action after cracking of cement matrix*

2.3.1 *Outline of modeling*

Short fibers with the specific length were randomly arranged in elements assuming the specimen size to be analyzed, so as to attain the specified fiber content by volume. As shown in Figure 2, a zero-size spring was placed on a point, where a fiber crosses two elements boundary, and the bonding stress of the fiber was acted on the spring. The embedment length l' and the angle to the normal direction to crack plane (orientation angle) ϕ were also calculated for each fiber. Note that the orientation angle was determined from the inner product of the normal vector and the vector in the direction of fiber orientation.

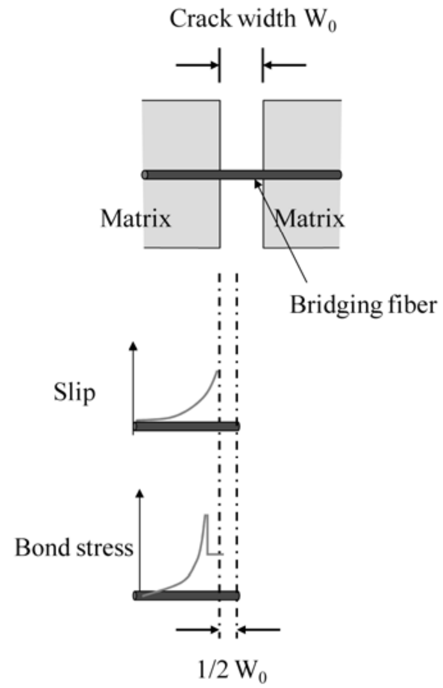

Figure 3. Pullout displacement obtained from crack width (before softening in pullout behavior).

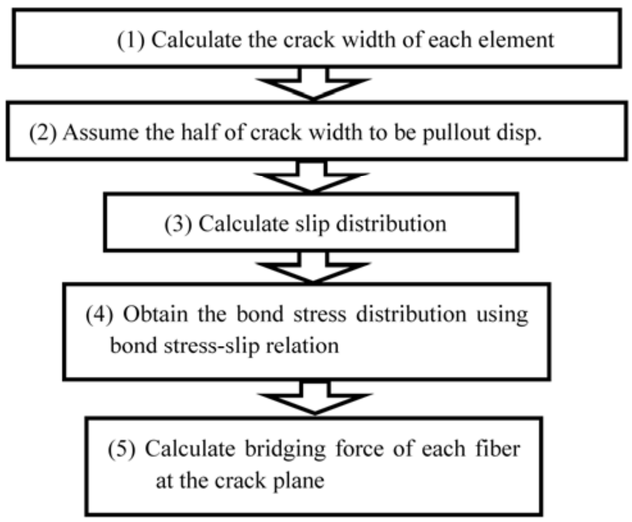

Figure 4. Procedure for calculation of fiber bridging force.

After cracking, the stress transfer by fibers across a crack plane in the cement matrix (hereafter referred to as "the matrix") was calculated by the steps shown in Figures 3 and 4 (Kunieda et al. 2008). Half of the calculated crack width W_0 was assumed to be the length of fiber pull-out displacement before softening of bond stress slip relation. After the softening, it was also assumed that the fiber having shorter embedment length was pulled out. Pull-out displacement was assumed to be equal to total crack width. The shape of slip distribution was determined through the analysis of single fiber pull-out tests. If the shape of slip distribution is known, then the bond stress distribution is determined from the bond stress-slip relationship. The bridging forces of fibers across cracks can then be calculated by integrating the bond stress distribution in the direction of the fiber axis. Uniaxial bond stress-slip curve as shown in Figure 5 was identified through the results of single fiber pull-out tests (Kozawa et al. 2008). Note that the water to binder ratio (W/B) of used matrix was 0.18, and high strength Polyethylene (PE) fiber was used in the tests.

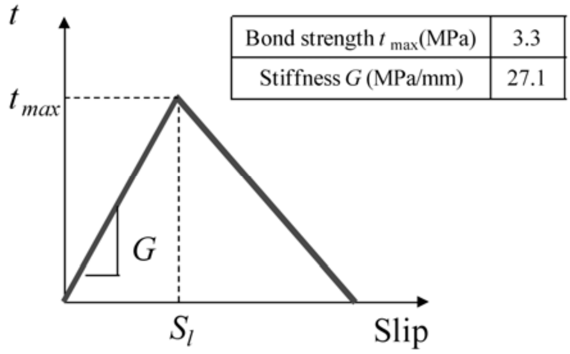

Figure 5. Bond stress-slip relation (PE fiber, W/B=0.18).

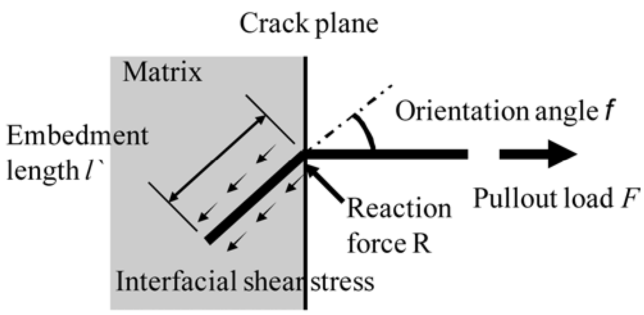

Figure 6. Bridging of inclined fiber to crack plane.

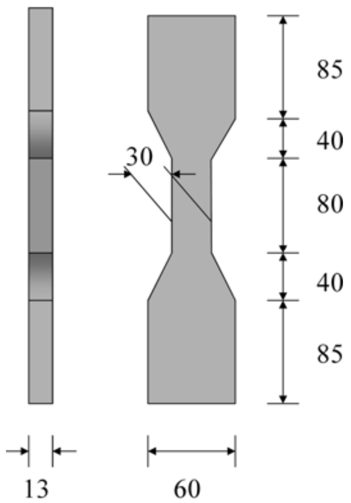

Figure 7. Shape of dumbbell-shaped specimen.

Eventually, normal force to crack plane due to bridging of fibers was modeled. However, the effect of cracking on section shear resistance is not considered.

2.3.2 *Increase of bond strength due to orientation angle*

As shown in Figure 6, a fiber was not always arranged perpendicular to crack plane, that means the fiber has orientation angle ϕ. Li et al. (1990) revealed the increase of bond strength in the inclined fiber pull-out test, and derived the following Equation;

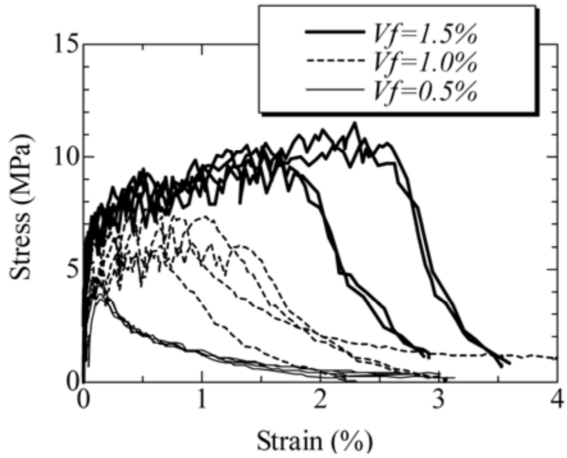

Figure 8. Tensile stress-strain curves of specimen with different fiber content.

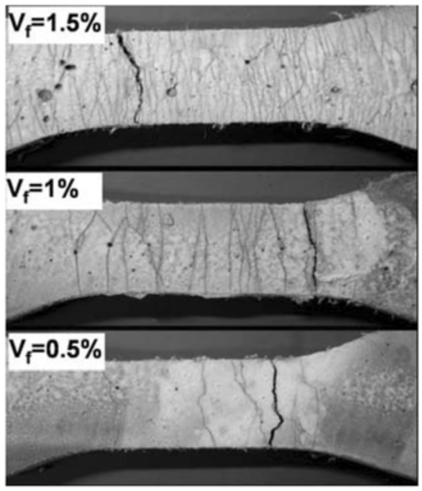

Figure 9. Final crack patterns after tensile tests.

$$F = F_0 e^{f\phi} \tag{2}$$

where F = pull-out load (N), F_0 = pull-out load at an orientation angle of 0 rad.(N), ϕ = orientation angle of fiber (rad.), f = parameter on snubbing effect. Regarding the parameter f, 0.5 was identified through numerical results (Kozawa 2009).

2.3.3 *Decrease of rupture strength of fiber due to orientation angle*

There are experimental findings that the rupture strength of fiber tends to be lower than the values given in the manufacturer's catalogue in the case of PVA fiber (Kanda & Li 1998). The orientation angle of each fiber to the crack plane affects rupture strength of fiber itself, as described in the following Equation;

$$\sigma_{fu} = \sigma^n{}_{fu} e^{-f'\phi} \tag{3}$$

where σ_{fu} = rupture strength of fibers (MPa), $\sigma^n{}_{fu}$ = apparent rupture strength at an orientation angle of 0 rad.(MPa), ϕ = orientation angle of fiber (rad), f' = strength reduction factor. In the previous research with PVA fibers, 0.3 was adopted as a f' value.

It has also been experimentally confirmed that the pull-out of fiber was observed in the case of PE fiber having ultra high strength. In this study, the apparent fiber strength value was used for the analysis.

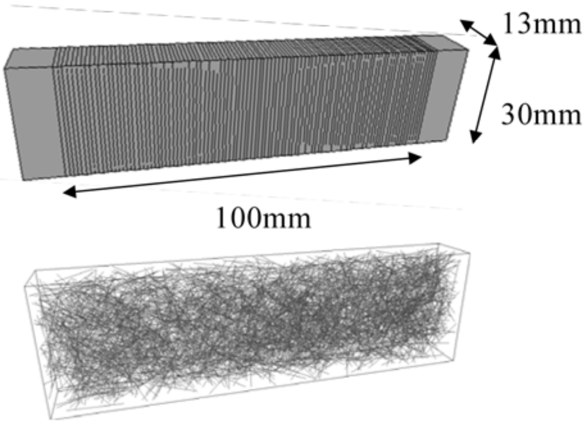

Figure 10. Discritized cement matrix and fibers.

3 ANALYSIS FOR CRACKING OF COMPOSITES WITH STRAIN HARDENING

3.1 *Outline of material response for analysis*

The target of this analysis is Ultra High Performance-Strain Hardening Cementitious Composites (UHP-SHCC) developed by Kunieda et al. (2007) and Kamal et al. (2008). The material exhibits high strength over 8MPa in tension, high strain capacity in tension more than 2%, with extremely higher durability. Uniaxial tensile tests of specimens containing 0.5%, 1.0% and 1.5% PE fibers (6 mm in length and 0.012 mm in diameter) were carried out. As shown in Figure 7, dumbbell-shaped specimens having a cross-section of 30 x 13 mm were used in the tests to measure the strain of the test zone 100 mm in length.

Table 1. Material properties for analysis.

Fiber	Length L_f(mm)	6
	Diameter d_f(mm)	0.012
	Elastic modulus E_f(GPa)	88
	Apparent strength $\sigma^n{}_{fu}$(MPa)	2700
	Volume fraction V_f(%)	0.5, 1.0, 1.5
Matrix	Elastic modulus E_m(GPa)	37.8
	Fracture energy G_{ft}(N/m)	20
Interface (bond)	Chemical bond strength τ_{max} (MPa)	3.3
	Stiffness G (MPa/mm)	27.1

3.2 *Outline of analysis*

The analysis models, which are discretization of cement matrix and fibers including an interface, are shown in Figure 10. The test zone measuring 30 x 13 x 100 mm was taken out of the specimen for the modeling, and the strain was determined in the area 100 mm in length similarly to the experiment. When using a RBSM, the crack pattern, which governs the strain capacity directly in this study, is affected by the mesh size and shape. For simplicity, however, the rectangle-shaped element was used and the mesh size was 1 mm in the direction of the longitudinal axis of the specimen, which is less than experimental crack spacing, and 13mm in the depth direction, so as to shorten the calculation time (a two-dimensional-like division). Fibers were modeled by randomly dispersing them in the specimen as shown in Figure 10. As for the boundary conditions, forced horizontal displacement was given to the right side element, while completely fixing the left side element of the specimen.

Table 1 gives the physical properties of the fibers, matrix, and fiber-matrix interface for the analysis.

3.3 *Trial analysis for specimen with different fiber contents*

Figure 11 shows the stress-strain relationship when the tensile strength of the matrix was assumed to be 7.5MPa. The tensile strength was determined through the flexural strength test of matrix itself, in which the flexural strength was 7.5MPa. The experimental results are also represented in the figures.

In the case of 0.5%, the first crack occurred at stress of 7.5MPa, and stress increases up to 3MPa after sudden drop in stress. Finally, softening behavior was observed. In this case, total response can be well simulated.

This model also predicts the softening behavior in the case of 1.0%, although experimental results shows slightly strain hardening up to 1.0% in strain.

Regarding the analytical result for 1.5% case, the analysis reproduced the repeated stress gains and losses beginning after the first crack onset and the large ultimate tensile strain exceeding 5%, although the test results showed only strain capacity ranging from 2.0% to 2.5%. No increases in the stress up to the point of 2.0% in strain were observed because of cracking strength of 7.5MPa. After that, it exhibits strain hardening up to 5.2% in strain. The total response cannot be simulated quantitatively. Figure 12 shows analytical crack patterns at strain of 1.0%, 2.0% and 4.0%, respectively. In strain hardening materials with multiple fine cracks, number of cracks strongly affects the strain capacity in tension. As shown in crack patterns of this analysis, most interfaces of elements, which were corresponding to cracks potentially, were opened, and it was induced constant crack spacing in each strain level. It seems that this behavior gave much strain values in the analysis.

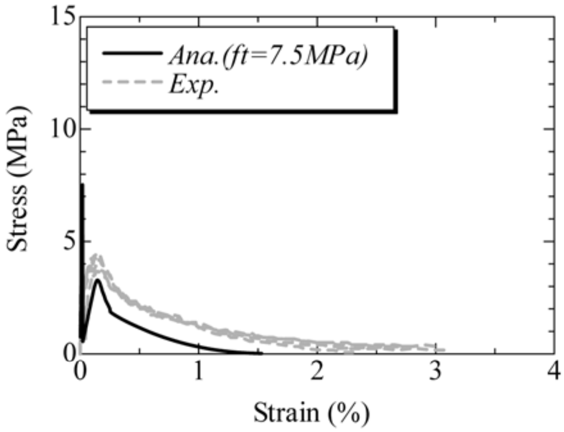

(a) Fiber content of 0.5%

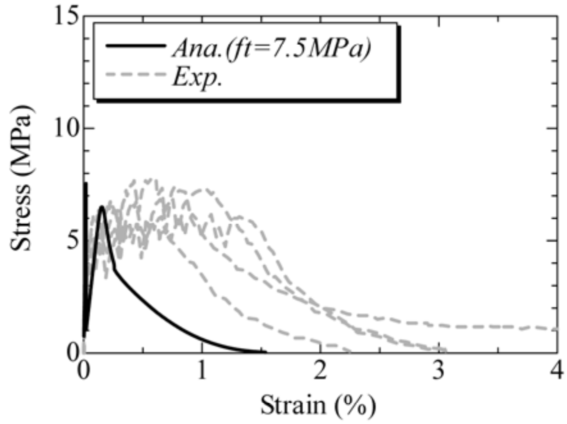

(b) Fiber content of 1.0%

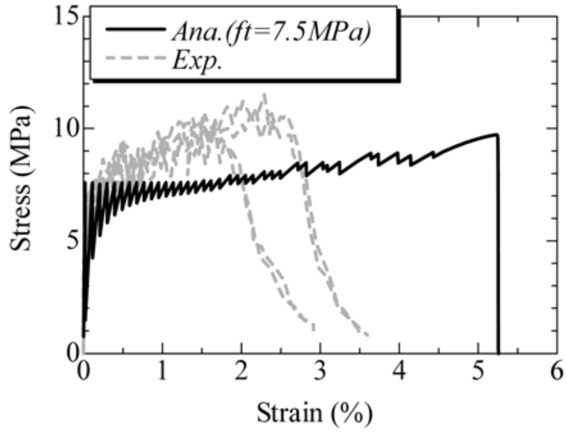

(c) Fiber content of 1.5%

Figure 11. Stress-strain curves of specimen with different fiber content.

(a) 1.0% in strain

(b) 2.0% in strain

(c) 4.0% in strain

Figure 12. Analytical crack patterns (1.5% case).

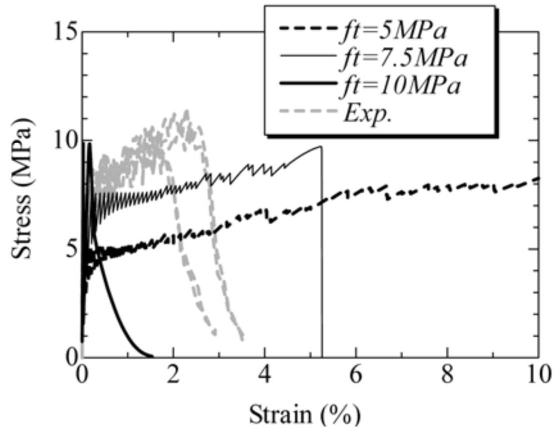

Figure 13. Effect of matrix strength (1.5% case).

In each case, stress value just before localization (failure) in the experiment was roughly simulated by the analysis. This means that fiber bridging strength, which controls the strength of composite in this material, is also evaluated in each series, and the modeling in this study is appropriate in terms of fiber bridging response. However, total response represented by stress strain curves was not simulated quantitatively. One of the reasons is existing materials has distribution of strength of matrix and fiber orientation etc, these cause sequential cracking within a specimen. In the following section, parametric studies related to distribution of matrix strength and fiber distribution were conducted.

4 PARAMETRIC ANALYSIS

4.1 *Effect of matrix strength*

Figure 13 shows the analytical results with different matrix strength, especially in the case of fiber content of 1.5%. Three kinds of matrix strength (5.0MPa, 7.5MPa and 10MPa) were adopted as a main parameter. As shown in Figure 13, as the matrix strength became lower, the strain capacity became higher with strain hardening behavior. Because the fiber bridging strength was less than 10MPa in the case of 1.5%, it seems that matrix strength lower than 10MPa is required to exhibit significant strain hardening behavior.

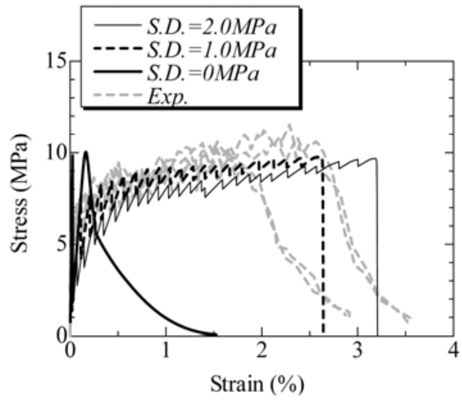

Figure 14. Effect of distribution of matrix strength (1.5% case).

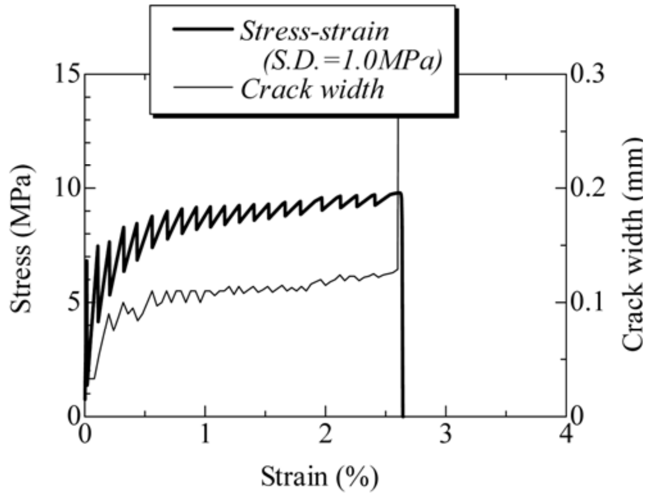

Figure 15. Changing of crack width up to final failure (1.5% case).

4.2 *Effect of distribution of matrix strength along specimen axis*

Figure 14 shows the analytical results with different property of matrix. Note that distribution of matrix strength along the specimen axis is assumed to be normal distribution, and three kinds of standard deviation (S.D.=0MPa, 1.0MPa and 2.0MPa) were analyzed under the averaged strength of 10.0MPa.

The result with S.D. of 0MPa showed only two cracks, because stress reached up to 10MPa twice, as described in previous. After that, softening behavior was observed. However, considering standard deviation (S.D.) changed fracture process dramatically from strain softening to strain hardening, as shown in Figure 14. In a physical behavior, first crack occurs at weakest cross section in a specimen, and second crack occurs at secondly weak cross section. Sequential cracking along specimen axis seems to be strongly affected by distribution of matrix strength. Regarding analytical results, larger standard deviation of matrix strength produced higher strain capacity in this analysis, under the assumption of constant bridging strength of fiber.

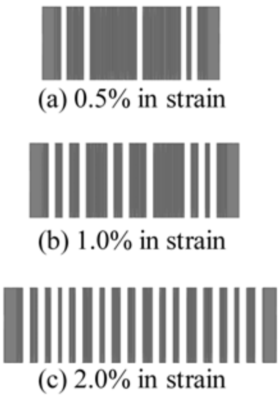

Figure 16. Crack patterns of specimen considering distribution of matrix strength (1.5% case).

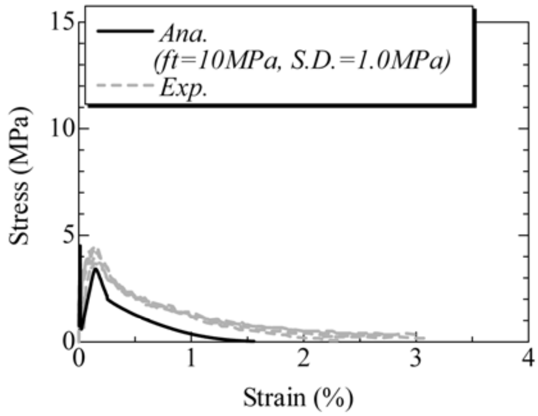

(a) Fiber content of 0.5%

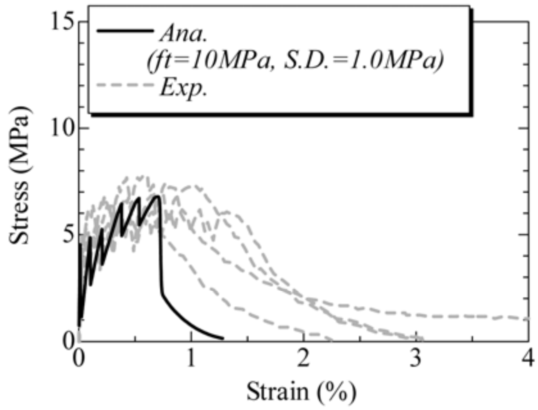

(b) Fiber content of 1.0%

Figure 17. Stress strain curves considering standard deviation of matrix strength.

Table 2. Averaged number of fibers in a cross section and its standard deviation.

	Averaged number of fibers in a cross section	Standard deviation
Case1	28830	152
Case2	28858	1565
Case3	28834	3196

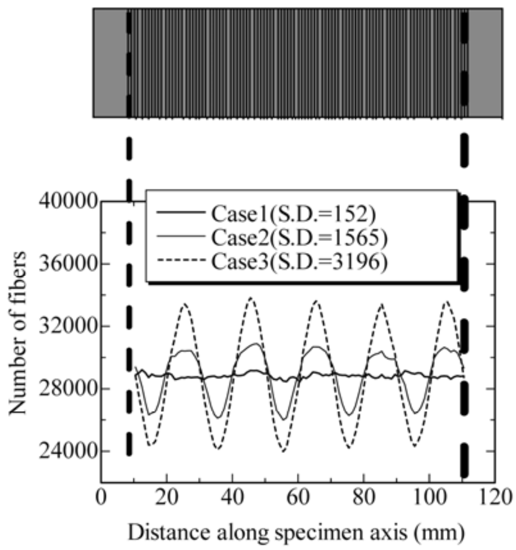

Figure 18. Number of fibers along specimen axis.

Figure 15 shows averaged crack width during fracture process in the case of 1.5% case. The analytical model simulates steady state cracking behavior that means no significant increase of crack width up to final fracture, and this behavior is similar to experimental trend (Li 2003).

Figure 16 shows crack patterns in the case of 1.5% with S.D.=1.0MPa. Although previous analysis without considering of S.D. of matrix strength indicated constant crack spacing as shown in Figure 12, the analysis considering S.D. of matrix strength shows non uniform crack spacing in each step because of randomly distributed matrix strength along specimen axis.

Based on this concept considering distribution of matrix strength, different fiber content case can be also simulated. Especially, slightly strain hardening shown in Figure 17(b) was reproduced, while the previous analysis estimated softening behavior of 1.0% case, as shown in Figure 11(b).

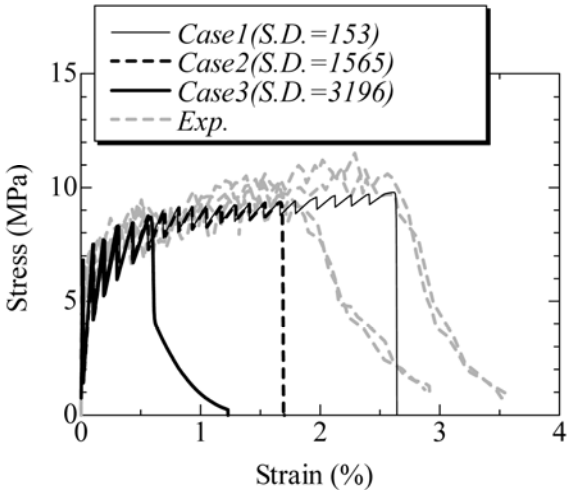

Figure 19. Stress stain curves of specimens with different fiber distribution.

4.3 *Effect of fiber distribution along specimen axis*

In order to assess the effects of fiber distribution in the specimen, analysis was conducted by changing the standard deviation of number of fibers across the each cross section, which is corresponding to potentially crack plane. In this model, each fiber is randomly positioned within the specimen, and averaged number of fibers across each cross section was about 28,800, as tabulated in Table 2. Three kinds of analysis with different standard deviation of number of fibers in each cross section (SD=0, 152, 1565 and 3196) were conducted, as shown in Figure 18. Figure 19 shows the stress-strain relationship of the specimens having different fiber distribution. The analytical results show that larger distribution of fiber having cross section with less fiber significantly reduces strain capacity.

Since less fiber imparts decreasing of bridging strength at a cross section to a composite, reduction of not only strain capacity but also ultimate strength was observed as shown in Figure 19.

5 CONCLUSIONS

In this study, a three-dimensional analysis method with discretized short fibers was assessed through the analysis of high strength strain hardening cementitious composites (UHP-SHCC). The findings obtained include the following:

(1) By analysis conducted on a material with high strength strain hardening and multiple fine cracks in tension (UHP-SHCC), this model roughly simulated mechanical response represented by stress strain curves and crack pattern.

(2) Parametric analysis was conducted to interpret fracture mechanism of strain hardening and multiple fine cracks in UHP-SHCC. Strain capacity was increased due to larger distribution of matrix strength. Strain capacity, however, decreased with increasing of distribution of fiber.

The authors intend to enhance the model so as to be useful for the development of fiber reinforcing materials.

REFERENCES

Bolander, J.E. & Saito, S. 1997.Discrete modeling of short-fiber reinforcement in cementitious composites, *Advanced Cement Based Materials*, 6, 76-86.

Bolander, J.E. & Berton, S. 2004. Cohesive Zone Modeling of Fracture in Irregular Lattices, Fracture Mechanics of Concrete Structures, *Proc. of FRAMCOS-5*, 989-994.

Cox, H. 1952. The Elasticity and Strength of Paper and Other Fibrous Materials, *British J. of Applied Physics*, 3.

Kamal, A., Kunieda, M., Ueda, N. & Nakamura, H. 2008. Evaluation of Crack Opening Performance of a Repair Material with Strain Hardening Behavior, *Cement and Concrete Composites*, 30(10), 863-871.

Kanda, T. & Li, V. C. 1998. Interface Property and Apparent Strength of High-Strength Hydrophilic Fiber in Cement Matrix, *Journal of Materials in Civil Engineering*, ASCE, 10(1), 5-13.

Kawai, T., 1978. New Discrete Models and Their Application to Seismic Response Analysis of Structures, *Nuclear Engineering Design*, 48, 207-229.

Kozawa, K. 2009. Study on Tensile Fracture Mechanism of Ultra High Performance-Strain Hardening Cementitious Composites and Its Modeling, *Master Thesis of Nagoya University*. (in Japanese)

Kunieda, M., Denarié, E. Brühwiler, E &Nakamura, H. 2007. Challenges for Strain Hardening Cementitious Composites – Deformability Versus Matrix Density, *Proc. of the fifth International RILEM Workshop on HPFRCC*, 31-38.

Kunieda, M., Kozawa, K., Ueda, N., Nakamura, H. & Ogura, H. 2008. Three-dimensional Meso-scale Analysis for Strain Hardening Cementitious Composites, Creep, Shrinkage and Durability Mechanics of Concrete and Concrete Structures, *Proc. of CONCREEP8*, 745-751.

Kozawa, K., Kunieda, M., Kanda, T. & Nakamura, H. 2008. Bond Properties of Organic Fiber Embedded in Ultra High Strength Matrix, *Proceedings of the Japan Concrete Institute*, 30(1), 231-236. (in Japanese)

Li, V.C., Wang, Y. & Backer, S. 1990. Effect of Inclining Angle, Bundling, and Surface Treatment on Synthetic Fiber Pull-out from a Cement Matrix, *Composites*, 21(2), 132-140.

Li, V.C. 1993. From Micromechanics to Structural Engineering –The Design of Cementitious Composites for Civil Engineering Applications, *Journal of Structural Mechanics and Earthquake Engineering*, JSCE, 10(2), 37s-48s.

Li, V. C. 2003: On Engineered Cementitious Composites(ECC) –A Review of the Material and Its Applications, J. of Advanced Concrete Technology, 1(3), 215-230.

Thomure, J. & Bolander, J.E. & Kunieda, M. 2001. Reducing Mesh Bias on Fracture within Rigid-Body Spring Networks, *Journal of Structural Mechanics and Earthquake Engineering*, JSCE, No.682/I-56, 15-23.